Journal of Applied Science, Engineering, Technology, and Education *ISSN: 2685-0591 (online)*
Vol. 4 No. 1 (2022)
https://doi.org/10.35877/454RI.asci615

Analysis of Hot-Air Supplemented Solar Drying Using Computational Fluid Dynamics Technique

Taiwo Aduewa* & Oyerinde Ajiboye Solomon

Department of Agricultural and Environmental Engineering, Federal University of Technology, Akure, 340252, Nigeria

Abstract

Energy is a crucial input in the process of economic, social and industrial development of any nation. Fluctuating solar insolation and late sunrise hour has led to poor quality dried biological material production. A simulation of hot-air supplemented solar dryer (HSSD) designed for such purpose is presented for temperature distribution based on direct solar irradiation of 1423 W/m2 of Akure, Nigeria (5.304º Latitude 7.258º Longitude). The environmental conditions in the hybrid dryer were measured during a day of operation. The model of the dryer was created and a numerical model was established to allow replicating the internal environmental conditions of the dryer. The airflow, temperature, radiative heat flux and other parameters inside the HSSD system were simulated using computational fluid dynamics (CFD) approach. The simulated result was compared with the calculated and estimated parameter values for the HSSD. The simulated air-flow pattern and temperature distribution on the horizontal and vertical planes in the drying chamber were analyzed and the results revealed spatial homogeneity of drying air condition. However, there is higher velocity profile at the outlet vent due to buildup of hot air at outlet vent. There was relatively low interference of external temperature in the drying chamber.

Keywords: Type your keywords here; between 3 and 6; separated by semicolons.

Received: 1 November 2021 Revised: 15 December 2021 Accepted: 16 January 2022

1. Introduction

The use of solar energy in recent years had reached a notable edge. The continuous research for an alternative power source due to the perceived instability of electricity, cost, scarcity and environmental hazards caused by fossil fuel burning is its driving force (Perera, 2018; Epstein et al., 2011). It had become even more popular as the continues to rise. Sun as energy source is known for its abundant in tropical countries which Nigeria is one with clear sunny skies of about 9 hs daily (Adeyoyin et al., 2019). With very few exceptions, the developing countries are situated in climatic zones of the world where the insolation is considerably higher than the world average of 3.82 kWh/m2 day (Akinboro et al.; Duffie and Beckman 2006).

Of all the available renewable energy sources, solar energy is the most abundant and available in both direct as well as indirect forms (Niebling, 2017) Recently, the use of hybrid solar dryer is gaining more attention of the farmers and food processors because it is relatively cheap with better quality output (Owusu & Asumadu-Sarkodie, 2016). The modes of conversion of energy from the sun determine the operational temperatures which has effect on the working efficiency, selection of material and ensure forecast and prediction of expected result in real life situation (IRENA 2018; Hertwich et al. 2014). For this reason, the implementation of Computational Fluid Dynamics (CFD) models as a tool which allows to know the internal behavior of hot-air supplemented solar dryer for optimal design output. Also, the implementation of solutions based on the results obtained according to the established numerical models (Alonge & Obayopo, 2019). According to Garduño-García et al. (2017), various design conditions can be evaluated within a virtual environment, reducing the number of experimental tests, allowing to evaluate spatially and temporally parameters such as pressure, temperature and air velocity, wall heat transfer coefficient, wall radiative heat flux, wall adjacent temperature contour, wall shear, inner wall temperature and eddy viscosity.

The present study seeks to analyze the fluid-dynamic behavior in the interior of the HSSD using CFD based on Reynolds-Averaged Navier-Stokes (RANS) equations in order to generate recommendations that increase the

* Corresponding author.
E-mail address: aduewataiwo@gmail.com

efficiency of the drying process based on some boundary conditions and material selected, leading to reduction in drying period and therefore the economic and labor savings. These simulated results generated were compared with selected calculated results derived from the design of the machine.

2. Methods and Simulation

2.1. Description of designed hot-air supplemented solar dryer

The designed HSSD consists of two main sections (solar dryer and the solar panel system). The dryer consists of three main compartments they are: the drying chamber, the solar collector and the hot-air chamber, while the solar panel system consists of the PV panel, battery and the charge controller. The dryer intends to maximize the use of energy available from the sun directly on the solar collector and also coupled with the hot air derived from the electric filament and axial fan to hasten which has its power source from the energy stored by the battery from the PV panel in order to ensure a faster, steady, stable and continuous rate of drying. The pictures of the automated hot air supplemented solar dryer and the major compartments can be seen in Figures 1 and 2. The selected designed parameters, formula and result for the hot-air supplemented solar dryer used for comparison with the simulated results for the purpose of analysis and understanding of the effect of simulation as basis for design accuracy, machine sensitivity analysis and production cost reduction is represented in Table 1.

Figure 1: Solar powered hot-air supplemented dryer

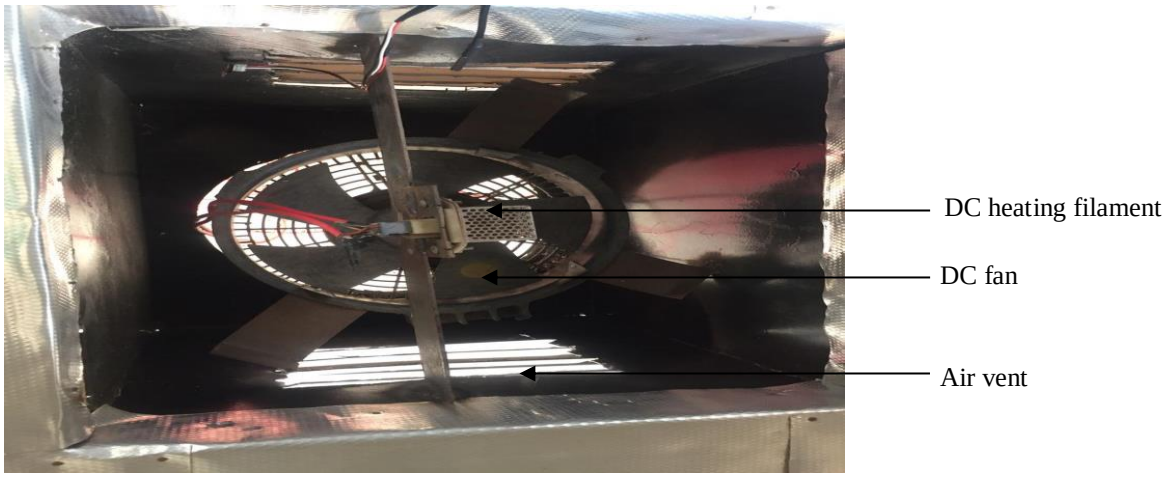

Figure 2: Hot-air supplement section of the dryer

Table 1: Designed parameters, formula and result

No	**Parameter**	**Formula**	**Result**
1	Mass of air required to remove moisture	$M_a = \frac{m_w}{\Delta w_{CB} \times n}$	0.436 kg/s
2	Total heat energy	$E = m_a(h_i - h_f)t_d$	139.498 MJ
3	Heat losses from the solar collector	$I_c A_c \tau_\alpha = Q_u + Q_l + Q_s$	Q_l = 216.9 W
4	Pressure drop through the drying chamber	$\Delta P_T = 6(2\Delta PB)$	ΔP_T = 1.0123 Pa
5	Radiation coefficient from plate to glass cover	$h_{rpc} = \frac{\sigma \times (T_p^2 + T_c^2) \times (T_p + T_c)}{\left(\left(\frac{1}{Ep}\right) + \left(\frac{1}{Ec}\right) - 1\right)}$	h_{rpc} = 7.879 $Wm^{-2}K^{-1}$
6	Radiation coefficient from cover to surface	$h_{rcs} = \in_c \times \sigma \times (T_c^2 + T_s^2) \times (T_c + T_s)$	h_{rcs} = 6.389 $Wm^{-2}K^{-1}$
7	Convection coefficient between plate and cover	$G_r = g \cdot \beta (T_b + T_c) L^3 / \upsilon^2$	h_{pc} = 3.06 $Wm^{-2}K^{-1}$
8	Convective heat transfer coefficient for air blowing over the cover	$q_{ca} = h_w = h_{cs} \cdot (T_c - T_s) + \Sigma_c \cdot T_c^4 - \Sigma_c L$	q_{ca} = 44.4 W/m^2K
9	Top loss coefficient	$U_T = \frac{1}{\left[\frac{1}{h_{rpc}+h_{pc}} + \frac{1}{h_w + h_{rcs}}\right]}$	U_T = 9.00 W/m^2K
10	Bottom loss coefficient	$U_b = \frac{k_i}{x_i}$	U_b = 0.8 W/m^2K
11	Bottom loss coefficient at the edge	$R_{p-e} >> R_{e-a} \rightarrow (UA)edge \cong \frac{k}{L_{edge}} A_e$	U_e = 0.675 W/m^2K
12	Total loss	$U_{total} = U_t + U_b + U_e$	U_{total} = 10.45 W/m^2K
13	Total solar radiation energy	$\Sigma I_t A_c = \Sigma \frac{Q_{co}}{E_c}$	$\Sigma I_t \cdot A_c$= 6.59065 kJ

E: Total heat energy, (kJ); m_a: Mass flow rate of air (kg/h), h_f: final enthalpy, (kJ/kg_{da}); h_i: initial enthalpy, (kJ/kg_{da}); t_d: drying time, (hr); A_c: Total collector area, (m^2), h_{rpc}: heat transfer coefficient (from plate to glass cover); h_{rcs}: heat transfer coefficient (from cover to surface); U_b: Bottom loss coefficient, K_i: insulation thermal conductivity; X_i: insulation thermal thickness; T_p: Absorber plate temperature (K); T_c: Glass cover temperature (K); T_s: hot air temperature (K); ΔPT = Total pressure drop through the dryer; R = Gas Constant; Ep = Emittance of coating (cellulose black paint) on absorber plate; Ec = Emittance of glass cover; h_w: heat transfer coefficient for wind blowing over the cover; σ = Stefan Boltzman Constant; g = acceleration due to gravity (m/s^2); L = Spacing (cm); υ = kinetic viscosity; G_r = Grashof number; β = coefficient of thermal expansion; ΔP_T = Total pressure drop; $I_t A_c$ = Total solar radiation energy on the collector area (kJ); Q_{co} = Absorbed heat energy by collector (kJ); E_c = Collector efficiency

2.2. Mathematical model for simulation

The numerical simulations for the designed hot-air supplemented solar drying system were performed using the RANS equations. The continuity, momentum and energy equations were solved with κ-ω SST (Shear Stress Transport) turbulence model, as proposed by Furbo (2010). from the *k*- ω turbulence model, initially formulated by Wilcox (1993). Other turbulence models were tested and the κ-ω SST was the one that best fits the experimental data. The Boussinesq approximation was used for thermal buoyancy in the drying chamber and solar collector chamber. A grid independence solution analysis was performed, in order to find the correct mesh size as a compromise between accuracy and computational cost. The numerical simulations were performed using the ANSYS-CFD FLUENT 17.2 software package, which is a general purpose CFD package that includes a solver based on the finite volumes method for structured and unstructured grids.

The mass, momentum and energy conservation equations for the HSSD design are given in a general form as presented in equation 1 as postulated by Jitjack *et al*. (2016), which was modified to equation 2 and 3:

$$\frac{\partial \rho}{\partial t} + \vec{\nabla}.(\rho U) = 0 \quad (1)$$

$$\frac{\partial (\rho U)}{\partial t} + \vec{\nabla}.(\rho U \otimes U) = -\vec{\nabla} p' + \vec{\nabla}.\left(\mu_{eff}\left(\vec{\nabla} U\right)\right) + B \quad (2)$$

$$\frac{\partial(\rho h_{tot})}{\partial t} - \frac{\partial \rho}{\partial t} + \vec{\nabla}.(\rho U h_{tot}) = +\vec{\nabla}.\left(k\left(\vec{\nabla}T\right) + S_E\right) \quad (3)$$

In the above equations, B is the sum of body forces, where μ_{eff} is the effective viscosity accounting for turbulence, and $p^{'}$ is the modified pressure, simplified in expressions according to Tiwari *et al*. (2016) in equation 4 and 5 respectively.

$$\mu_{eff} = \mu + \mu_t \quad (4)$$

$$p' = p + \frac{2}{3}\rho k \quad (5)$$

h_{tot}, p and k represent the total specific enthalpy, the pressure and the thermal conductivity and S_E is the energy equation source term. The total specific enthalpy has a relationship with thermodynamic specific enthalpy h, as represented by equation 6 as stated by Tiwari *et al*. (2016).

$$h_{tot} = h + \frac{1}{2}U^2 \quad (6)$$

In this research, the effects of turbulence being the major characteristic parameter affecting temperature and air velocity flow are considered using the SST turbulence model. Menter *et al*. (2010), proposed this model and this equation has its origin from the denominated baseline *k*-ω model by Glushko *et al*. (2010). The baseline *k*-ω model utilizes the *k*-ε model in regions far away from the walls and the *k*-ω Wilcox model near the surface of the dryer. The SST model is a significant improvement of the baseline *k*- ω model, considering the transport of the turbulent shear stress by a limitation of the eddy viscosity v_t as presented in equation 7.

$$V_t = \frac{a_1 k}{max(a_1 w, SF_2)} \quad (7)$$

Where; $v_t = \mu_t/\rho$ and S represents an invariant measure of the strain rate. F_2 is a blending function, which restricts the limiter to the wall layer computed by equation 8 according to Menter *et al*. (2003).

$$F_2 = \tanh(arg_2^2) \quad (8)$$

with

$$arg_2 = max\left(\frac{2\sqrt{k}}{\beta' \omega'} \frac{500v}{y^2 \omega}\right) \quad (9)$$

The SST model is a two-equation model, which means that two additional transport equations must be solved: one for the turbulent kinetic energy κ and one for the specific dissipation ω, given, respectively, by equation 10 and 11 according to postulation presented by Beniaiche *et al*. (2018).

$$\frac{\partial(\rho k)}{\delta t} + \vec{\nabla}.(\rho U k) = \vec{\nabla}.\left[\left(\mu + \frac{\mu_t}{\sigma_{k3}}\right)\vec{\nabla}k\right] + P_k - \beta' \rho k \omega \quad (10)$$

$$\frac{\partial(\rho \omega)}{\delta t} + \vec{\nabla}.(\rho U \omega) = \vec{\nabla}.\left[\left(\mu + \frac{\mu_t}{\sigma_{\omega 3}}\right)\vec{\nabla}\omega\right] + (1 - F_2)2\rho \frac{1}{\sigma_{\omega 2}\omega}\vec{\nabla}k\vec{\nabla}\omega - \beta_3 \rho \omega^2 \quad (11)$$

The constants used in the SST model equations are defined according to Bentaleb *et al*. (2012), as: $\beta^{'}$ =0.09; α_1 =5/9; σ_{k1} =2; $\sigma_{\omega 1}$ = 2; σ_2 = 0.44 β_2 = 0.0828 α_{k2} = 1; α_{w2} = 1/0.856

The coefficients of the SST model are a linear combination of the corresponding coefficients of the underlying models, given by equation 12:

$$\Phi_3 = F_2 \Phi_1 + (1 - F_2)\Phi_2 \quad (12)$$

In the transport equations, P_k is the turbulence production tensor due to viscous forces, which is computed by Gatski & Bonnet (2013), at presented in equation 13:

$$P_k = \mu_t \vec{\nabla}U.\left(\vec{\nabla}U + \vec{\nabla}U^T\right) - \frac{2}{3}\left(\vec{\nabla}.U\right)\left(3\mu_t \vec{\nabla}.U + \rho k\right) \quad (13)$$

It is important to notice that the model definitions and formulation are presented as used in ANSYS-CFD FLUENT 17.2 version since the numerical simulations were performed with this commercial code.

3. Results and Discussion

3.1. Geometry

The geometry of the HSSD was created using Autodesk Inventor software version 2018.3 and exported to ANSYS-CFD FLUENT 17.2 software which is specifically designed for the creation and preparation for simulation. The simulation process of the HSSD consisted of dryer drying chamber, solar collector region and the hot-air supplement regions. The employed computational domain includes the dryer without the trays as shown in Figure 3. Each region was modelled as a fluid domain and then interfaced together using an option of domain interface during simulation. After the interface establishment, the complete model was exported for mesh development. The boundary conditions, material and other properties were set through parameterized case files. FLUENT solves the problem until either the convergence limit is met or the amounts of iterations specified are complete. The modelled mesh density for the HSSD was increased in the region around the collector plate and the centre region of drying chamber where large gradients exit. The total number of elements and nodes varied among the different simulations and was in the range of 2,186,624 elements and 419,267 nodes. The mesh in regions near the walls was refined using the inflated boundary conditions tool of ANSYS-CFD FLUENT 17.2 (Figure 4).

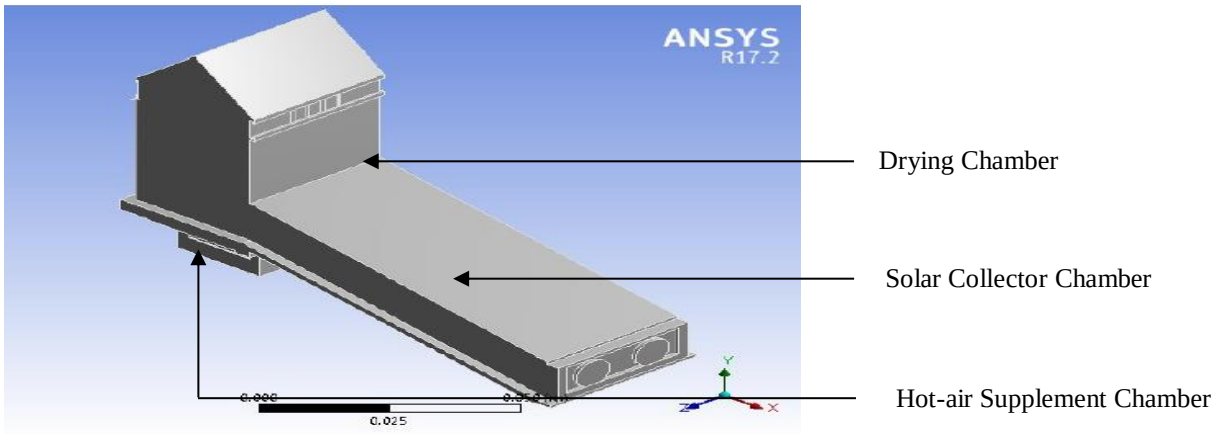

Figure 3: 3D model of hot-air supplemented solar dryer.

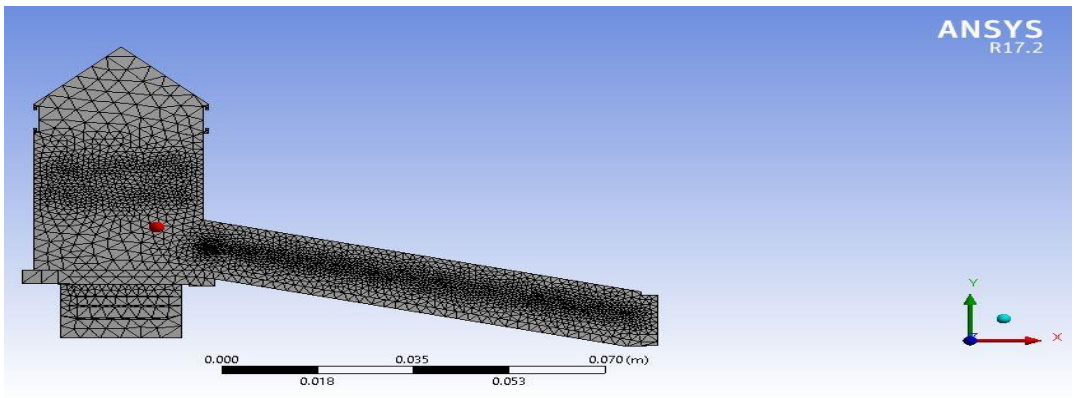

Figure 4: Surface mesh of the designed hot-air supplemented solar dryer.

3.2. Boundary conditions for the simulated HSSD

The numerical solution of the above equations involves the use of specific boundary conditions, in particular at surfaces bounding of the domain. In this study the boundary conditions were defined as function of the experimental data, as following:

Inlet: according to the experimental data, a mass flow rate of 0.01344 kg/s was selected at the entrance of the solar collector. The inlet velocity was set at 1.2 m/s with a turbulent intensity of 5 %. Direction of airflow was normal to air inlet. It was assumed that the air was at ambient temperature, equal to 26 °C.

Monte Carlo technique was used for the additional solar radiation modeling with directional radiation flux of 900 W/m^2 (Maximum Radiation flux for experimental location). At absorber plate the temperature was also set at 65 °C from the experimental data. The other walls were treated with the default boundary conditions of no slip, with smooth and adiabatic walls due to insulation.

Outlet: it was assumed a gauge pressure of 0 Pa at the outlet tube.

Walls: At the walls, no slip and impermeable boundary conditions were used. These conditions assume zero tangential velocity at the walls, and a zero gradient of the other parameters in the normal direction at the walls, except in some turbulence parameters. The temperature at the walls was set out considering the measured experimental values and applying a boundary condition of Dirichlet type. At the glass walls, the temperature was considered equal to 35 °C, and at the lower plate of the collector, the temperature was considered 57.5 °C, according to experimental data. At the other plates, an adiabatic condition was assumed (zero temperature gradient in the normal direction at the wall), due to the insulation used in the dryer. For the necessary turbulent quantities at boundaries the ANSYS-CFD FLUENT default boundary conditions assumed for each turbulence model were employed. The model's constants also were assumed as the default values considered in the ANSYS-CFD FLUENT code. The flow is simulating considering a steady state operating condition. The air inside the dryer was assumed as an ideal gas, with an ambient pressure of 97.121 Pa. This is a characteristic ambient pressure value for FUTA, Akure, where the dryer was installed.

3.3. Simulation result of drying system

The HSSD simulation was carried out in 3-dimensions to give the actual and detailed air flow in the dryer, in order to visualize the different condition as represented in the simulation results. The model solution in terms of streamlines, contours and vector plots at horizontal and vertical planes in the drying chamber was visualized using ANSYS CFD FLUENT. The criterion of convergence of variables associated with the momentum, heat transfer and turbulence was achieved maximum of 10 iterations for each time. The convergence associated with the turbulence model was reached suggesting that the implemented κ - ε SST (Shear Stress Transport) turbulence model, as proposed by Beniaiche *et al*. (2018), from the *k*- ω turbulence model, initially formulated by Wilcox, (1993); Gatski & Bonnet (2013), was appropriate.

The airflow, temperature, radiative heat flux and other parameters inside the HSSD system were simulated using the ANSYS software package. The designed drying system based on calculated values were employed in the design of the drying system. A three-dimensional model was developed to investigate heat transfer, relative humidity, air velocity in the drying system, temperature, wall heat transfer coefficient, wall radiative heat flux, pressure, wall adjacent temperature contour, wall shear, inner wall temperature and eddy viscosity in the hot-air supplemented solar dryer for drying and moisture removing process. The simulation was used to determine the Figures 5-13 showing the simulation model for different parameters.

Figure 5 presents the airflow temperature in a 3D view in the middle of the dryer (inlet section, solar chamber, drying chamber and vent region). It is established with simulation that the distribution of temperatures inside the dryer in this 3D view is almost homogeneous, except at the solar collector surface (bottom inclined surface), where higher temperatures are obtained, of about 56 °C, as well as, the highest temperature gradients. The surface receives more energy than the upper surface made from glass this was due to the thermal radiation absorption of the solar collector plate. At an average, the mean temperature gradient between the dryer inlet and outlet regions is approximately equal to 14 °C, which is in line with literatures of (Menter *et al*. 2003; Tarigan, 2018).

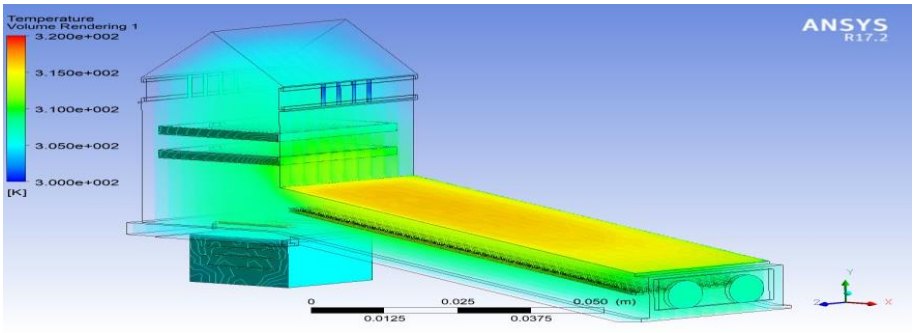

Figure 5: Temperature movement inside the drying system (axis x, y and z directions).

The value derived for air velocity in the drying chamber with simulation was around 0.75 m/s (Figure 6) given a closer result to the minimum air velocity required for drying agricultural crops which according to literature is between 0.8 to 1.2 m/s except for the upper vent area where there is a slight increase in the velocity value causing increased pressure due to smaller outlet for moisture laden air escape.

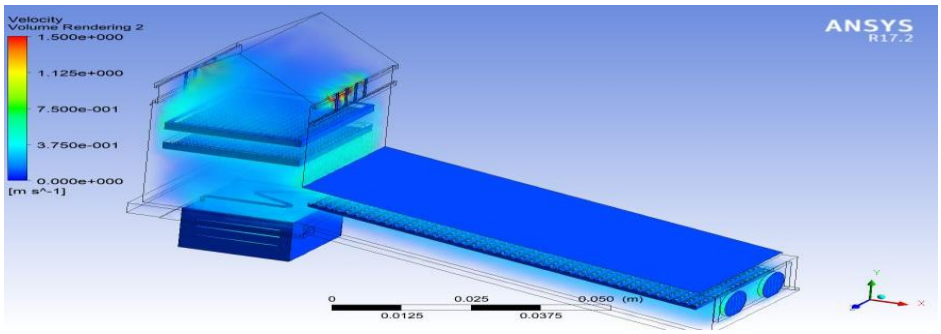

Figure 6: Air velocity distribution inside the drying system (axis x, y and z directions).

Heat loss coefficient for the flat plate collector due to radiation calculated numerically gave a result of 7.879 W/m^{2}K while that of simulation was lesser than 8.0 W/m^{2}K. Heat loss coefficient from cover to surface due to radiation calculated numerically gave a result of 6.389 W/m^{2}K while that of simulation was around than 10.0 W/m^{2}K which is still not far from the numerical value derived from calculation (See Figure 7).

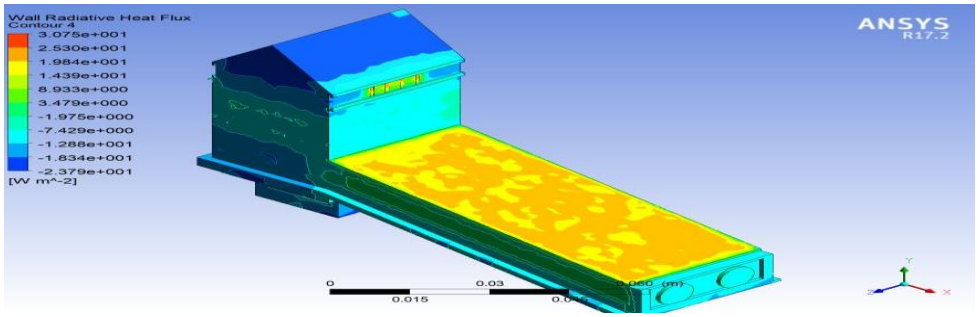

Figure 7: Wall radiative heat flux of the drying system (axis x, y and z directions).

Figure 8 shows the wall adjacent temperature simulation. This simulation result shows the temperature gradient as solar radiation reflects on the adjacent wall of the dryer external structure. The effect is equal to static temperature with the simulation node value switched off. With a lagging thickness of 5 cm, the temperature of the air immediately after the external wall was at a peak level of 51.75 °C around the solar collector and drying chamber wall. The glazing on the solar collector has adjacent temperature value range of 50.45 °C to 36.35 °C.

Figure 9 shows the temperature profile of the inner wall. The glazing temperature give the highest temperature level based on the presence of black body solar collector leaving the temperature at around. The profile increases

up the collector chamber and this phenomenon positively indicate the effect of angle of inclination with the upper section of the chamber having the highest. Likewise, at pre-set temperature of 50 °C, the temperature level in the dying chamber reduces upward as a result of minimal heat loss and also discharge via the upper vents.

The homogeneity of the dryer was shown in Figure 10. The 3-D view shows relatively low turbulence level in the drying system under same volume of air introduced by the two axial fans.

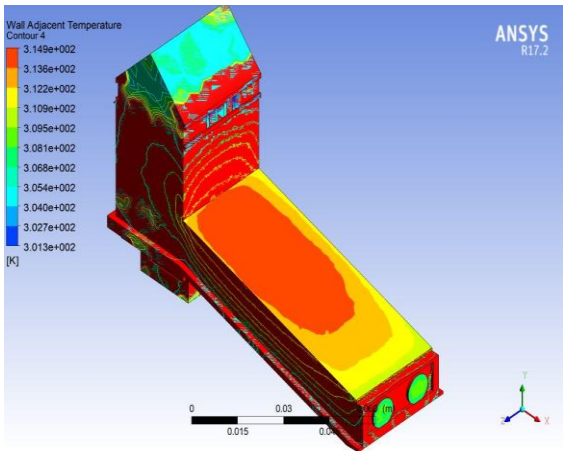

Figure 8: Wall adjacent temperature of the drying system

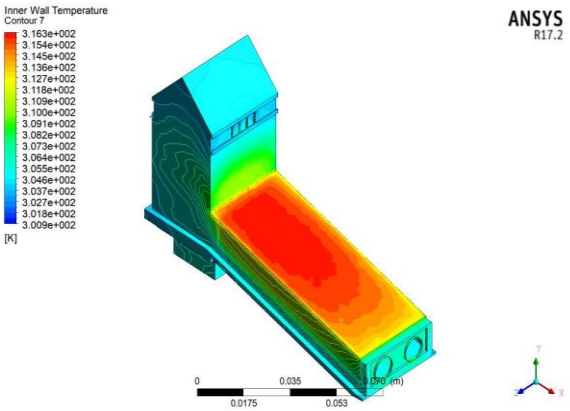

Figure 9: Inner wall temperature of the drying system

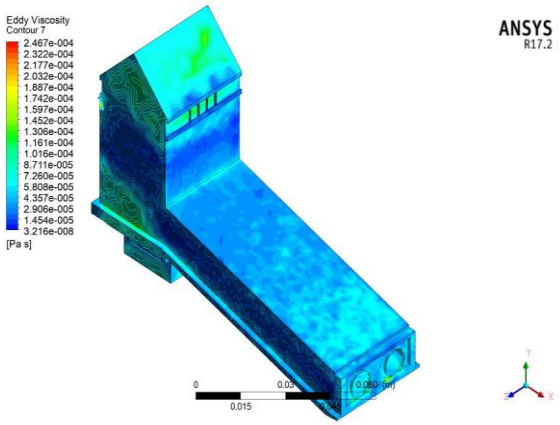

Figure 10: Eddy viscosity simulation of the drying system

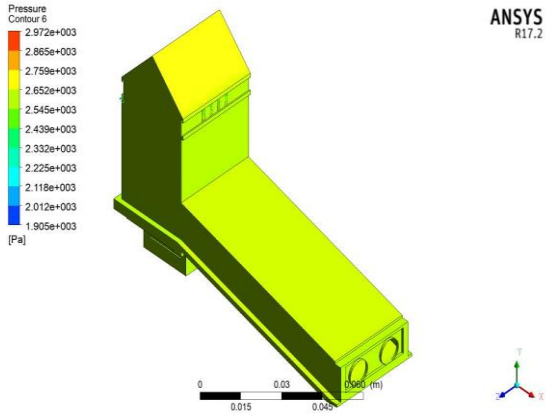

Figure 11: Pressure simulation

Figure 11 shows the pressure distribution within the drying system. The numerically estimated pressured drop for the system was 1.0123 Pa, which agrees with simulated result that ranges 2.4 Pa, inside the uncertainty range of the pressure sensors.

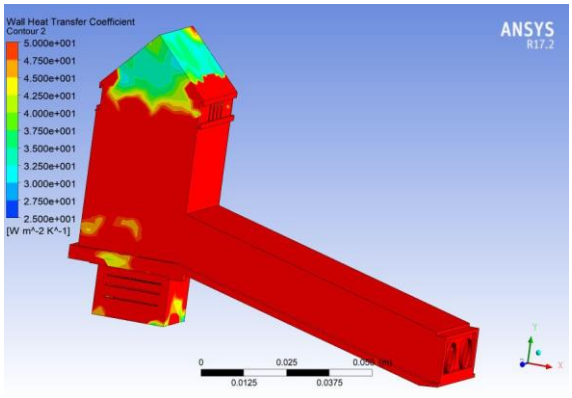

Figure 12: Wall heat transfer coefficient of the drying system

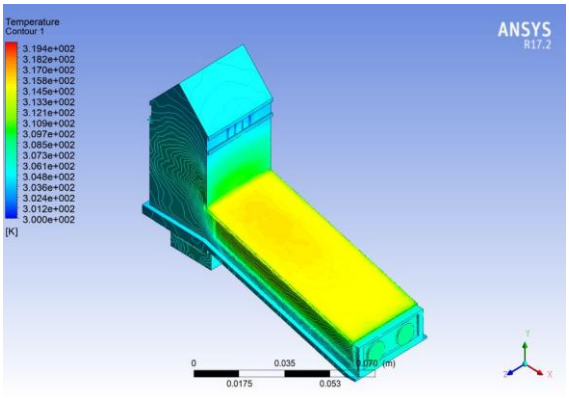

Figure 13: Temperature distribution inside the drying system

It can be seen in Figure 13 that, since the air enters the drying chamber at ambient temperature being heated by the solar collector before mixing up with the heat from the supplementary section, the temperature on the solar chamber walls increase towards the drying chamber. The wall temperatures are also in accordance with experimental data. The experimental value for the drying chamber wall is 40 °C. In the simulations, a temperature of 36 °C was obtained. It should be pointed out that these walls are well insulated in the experimental setup, and were simulated considering adiabatic wall in the numerical model. Thus, the comparison considers resultant temperature values, one experimentally determined and the other numerically computed. In this case it can be noted that the model reproduces well this wall temperature.

4. Conclusion

Hybrid solar dryers which HSSD is an example have proven to be successful in drying most agricultural produce. Since the laboratory experimentation takes long time and is not economical for the purpose of testing, using CFD it is very easy and economical to conduct the tests on the model and analyze the results without much investment of time and money. Based on simulation output it was obtained that the additional hot-air supplement compartment allows the continuous drying process at night and during wet seasons. This shortens the drying time and improves the quality of product to be dried. CFD simulation is useful in predicting air velocity and temperature profiles in a drying chamber. The result shows uniform temperature distribution of airflow throughout the dryer based on pre-set temperature. The temperature was maintained constant in the drying chamber due to additional heat source controlled by a thermostat. The velocity of airflow was homogeneous throughout the dryer. This behaviour is desirable and suitable for dryer purposes, since it guarantees a high-quality product and homogeneous drying process. The prediction of the airflow inside the dryer can assist to design the most suitable geometric configurations of other hybrid dryers and improve the drying process. Hence after analyzing the results with the help of CFD ANSYS package, the results obtained was satisfactory and seem practical. However further validation of these results can be done by conducting physical experimentation.

Conflicts of Interest: The authors declare that they have no conflicts of interest to report regarding the present study.

Contribution: **Aduewa**: Conceptualization, design, analysis, writing, concept and design, data acquisition, data analysis / interpretation, drafting manuscript, critical revision of manuscript, statistical analysis. **Solomon**: concept and design, data acquisition, data analysis / interpretation, drafting manuscript, critical revision of manuscript, statistical analysis, admin, technical or material support, supervision, final approval.

References

Adeyoyin, S. O., Alawiye, M. K., & Ewulo, O. R. (2019). Awareness and Use of Solar Energy as Alternative Power Source for ICT Facilities in Nigerian University Libraries and Information Centres. *Library Philosophy and Practice (ejournal).* 2372. 1-8.

Akinboro, F. G., Adejumobi, I. A., & Makinde, V (2013). Solar energy installation in Nigeria: Observations, prospects, problems and solutions. Transitional Journal of Science and Technology. 2(4):15-27.

Alonge, O. I., & Obayopo, S. O. (2019). Computational fluid dynamics and experimental analysis of direct solar dryer for fish. *Agricultural Engineering International: CIGR Journal*, 21(2): 108–117.

Beniaiche, A., Nadir, M., Cerdoun, M., & Carcasci, C. (2018). Effect of turbulence models' choice on the aero-thermal flow numerical validations within a ribbed trailing edge geometry. *Proceedings of the Institution of Mechanical Engineers, Part A: Journal of Power and Energy*. 233(1):52-77.

Bentaleb, Y., Lardeau, S., & Leschziner, M. A. (2012). Large-eddy simulation of turbulent boundary layer separation from a rounded step. *Journal of Turbulence*, 00(00), 1–26.

Perera, F. (2018). Pollution from Fossil-Fuel Combustion is the Leading Environmental Threat to Global Pediatric Health and Equity: Solutions Exist. *International Journal of Environmental Research and Public Health*. 15(1): 16.

Epstein, P. R., Buonocore, J. J., Eckerle, K., Hendryx, M., Stout III, B. M., Heinberg, R., Clapp, R. W., May, B., Reinhart, N. L., Ahern, M. M., Doshi, S. K., & Glustrom, L. (2011). Full cost accounting for the life cycle of coal in "Ecological Economics Reviews." Ann. N.Y. *Academy. Science*, 1219, 73–98.

Duffie A. J., & Beckman, W. (2006). Solar Engineering of Thermal Processes, 3rd Ed., John Wiley & Sons, Inc., New York. 435-441.

Ficarella, A., Perago, A., Starace, G., & Laforgia, D. (2003). Thermo-fluid Dynamic Investigation of a Dryer, using Numerical and Experimental Approach, *Journal of Food Engineering*, 59, 413-420.

Furbo, E. (2010). Evaluation of RANS turbulence models for flow problems with significant impact of boundary layers. Teknisk- naturvetenskaplig fakultet UTH-enheten, Hus. 1-55.

Garduño-García, A., López-Cruz, I. L., & Ruiz-García, A. (2017). Mathematical modeling of greenhouse solar dryers with natural and forced convection for agricultural products: state of the art. *Ingeniería agrícola y biosistemas*. 9(1):1-12.

Gatski, T. B., & Bonnet, J. (2013). Compressibility, Turbulence and High Speed Flow (Second Edition) Elsevier Ltd, Academic Press, Massachusetts, United States. 39-77.

Glushko, G. S., Ivanov, I. E., & Kryukov, I. A. (2010). Computational method for turbulent supersonic flows. *Math Models Computational Simulation* 2:407–422.

Hertwich, E., Honnery, D., Infield, D., Kainuma, M., Khennas, S., Kim, S., Nimir, H. B., Riahi, K., Strachan, N., Wiser, R., & Zhang, X. (2014): Energy Systems. In: Climate Change (2014). Mitigation of Climate Change. Contribution of Working Group III to the Fifth Assessment Report of the Intergovernmental Panel on Climate Change [Edenhofer, O., R. Pichs-Madruga, Y. Sokona, E. Farahani, S. Kadner, K. Seyboth, A. Adler, I. Baum, S. Brunner, P. Eickemeier, B. Kriemann, J. Savolainen, S. Schlömer, C. von Stechow, T. Zwickel & J.C. Minx (eds.)]. Cambridge University Press, Cambridge, United Kingdom and New York, NY, USA.

Irena (2018), Global Energy Transformation: A roadmap to 2050, International Renewable Energy Agency, Abu Dhabi. 8-40.

Jitjack K., Thepa, S., Sudaprasert, K., & Namprakai, P. (2016). Improvement of a Rubber Drying Greenhouse with a parabolic cover and enhanced panels. *Energy and Buildings* 124: 178-193

Menter, F. R., Kuntz, M., & Langtry, R. (2003). *Ten Years of Industrial Experience with the SST Turbulence Model, Turbulence, Heat and Mass Transfer* 4, edited by K. Hanjalic, Y. Nagano, and M. Tummers, Begell House, Inc.

Niebling, C. (2017), Adding Thermal Energy to State Renewable Energy Standards: Opportunity, Status, and Challenges, presentation at REV 2017, 2 October 2017, www.inrsllc.com/

Owusu, P. A., & Asumadu-Sarkodie, S. (2016). A review of renewable energy sources, sustainability issues and climate change mitigation, *Cogent Engineering*, 3(1):1-9.

Tarigan, E. (2018). Mathematical Modeling and Simulation of a Solar Agricultural Dryer with Back-Up Biomass Burner and Thermal Storage. *Case Studies in Thermal Engineering*. 12:149-165.

Tiwari, S., Tripathi, R., & Tiwari, G. N. (2016). Thermal Analysis of Photovoltaic Integrated Greenhouse Solar Dryer. *World Academy of Science, Engineering and Technology, International Journal of Electrical, Computer, Energetic, Electronic and Communication Engineering*, 10(1): 81-85.

Wilcox, D. C. (1993). *Turbulence Modeling for CFD*. 1st Edt. DCW Industries Inc., California.